An Improved Strategy for Torque Ripple Reduction of Dual Three-Phase Brushless DC Motor Fed by Two Diode-Clamped, Three-Level Inverters Using Model Predictive Control

Zahra Emami* and Abolfazl Halvaei Niasar*(C.A.)

Abstract: Multiphase electric motors are useful for industrial and military applications that need high power, fault tolerance control, smooth torque, and the ability to share power and torque compared to conventional three-phase electric motors. One type of Multiphase electric machine is Brushless DC Motors (BLDCM) which uses conventional strategies such as hysteresis current controllers. It has important challenges such as high torque ripple, low efficiency, vibrations, and noise that are undesirable for high power applications such as submarines. This paper proposes a new finite control set model predictive control (FCS-MPC) approach with reduction of computational for diode-clamped three-level (DC3L) inverter fed to dual three-phase BLDCM (DTP-BLDCM) by selecting optimal vectors to solve the above problems. Also, an approach of balancing the voltage of the capacitors in two of the DC3L inverters to reduce torque ripple has been proposed. The results of the suggested MPC method are contrasted and verified with the multiband hysteresis current (MHC) method through simulation. The simulation results specify that the suggested MPC controller works superior than the MHC controller. Also, due to the simplicity and low complexity of the suggested MPC strategy used, the real implementation possibility and performance of the controller are checked by simulations for a 4125-V/2.7-MW/350-RPM DTP-BLDCM.

1 Introduction

MULTIPPHASE electric motors are beneficial for industrial and military applications that require high power, smooth torque, fault tolerance, lower current stress for switching devices, and more degrees of freedom for control compared to traditional three-phase electric motors [1-3]. A type of motor that are very extensively used is dual three-phase (DTP) motors are the most prevalent due to the simple structure and efficiency of the drive system and superiority over three-phase motors.

Initially, this topology was executed only for powerful induction drives and then PMSMs and newly brushless DC motors (BLDCMs) [4-6]. In these motors, which are called (DTP-BLDCM) for short, the stator has two categories of three-phase windings with separate star connections, and the same windings in each group have a spatial phase difference of 30 degrees compared to each other [7].

In DTP motors with asymmetric configuration, due to mutual inductance between two sets of three-phase windings, extra current pulsations are created, which increases ripples of the electromagnetic torque. In some special applications such as the military, the motor torque ripple causes mechanical vibration or acoustic noise which is not acceptable according to military standards. Many control studies are based on (DTP-PMSM) such as field-oriented control (FOC) and direct

torque control (DTC) that using them cause considerable ripple electromagnetic torque in DTP-BLDCM. Moreover, BLDCMs have disadvantage such as commutation torque ripple that scholars have tried to solve this problem.

In [8], DTC strategy based on duty ratio for DTP motors is presented, which can significantly decrease the flux and torque ripples to a level with switching frequency capability, but this method does not have a good dynamic response. The FOC method is also an extended vector control method for multiphase motors. These types of motors require multiple subspaces for motor control and additional PI current controllers. Despite the good quality, this method needs difficult adjustment of the PI controller gains. Furthermore, the bandwidth of the current control loop limits the dynamic response [9]. Although hysteresis control method has fast current responses and good robustness, it has problems such as significant current in commutation times, torque ripple and variable switching frequency. Hysteresis strategies use hysteresis bands that the bandwidth of hysteresis controllers affects the control quality [10]. In addition, the number of sensors required in DTP-BLDCM control is an important issue. Some references have provided different solutions for this problem to decrease sensors by the DC link current measurement [11, 12].

Lately, finite control set model predictive control (FCS-MPC) strategy has been promoted for advantages including its flexibility in defining a control action, simplicity in implementation, fast transient response, and the option of adding restrictions for multiphase motor drives. In this strategy, the motor discrete model is applied to anticipate its variables to acquire the optimal switching states using the cost function to access optimal control [13, 14]. However, the MPC control method is mostly concentrated on three phase motors [15, 16] and use of MPC for six-phase motors induction Motor and DTP-PMSM has been less investigated and most importantly has been used for low powers and motors is fed using two-level inverters [17-19]. Furthermore, the discussed MPC strategies for multiphase motors still contain some challenges including heavy computational load and complex modulation process [13-19].

In the medium voltage (MV) drives of AC motors that are fed by PWM inverters, the voltage and current values are high. In [20] has described the types of inverters used for multi-phase motors. In [21, 22] presented examples of several commercial electric drives in several marine vessels, with drive power ranging from 0.2 MW to 81 MW. Most of these drives use three and five-level inverters. Hence, the diode-clamped three-level (DC3L) inverter is a suitable alternative compared with two-level inverters. Reduction of voltage stress on inverter switches and reduction of voltage harmonics applied to the motor and reduction of switching losses and less electromagnetic interference are advantages of these inverters [23-25]. Also, using of the FCS-MPC method of a DTP-BLDCM fed by two DC3L inverters needs 27×27=729 various voltage vectors that is calculated by the cost function in each control cycle. To reduce the complexity of FCS-MPC control, several studies have been done on DTP-PMSM. By reducing the computational load, the system efficiency increases and the sampling rate of the algorithm can be increased for lower torque ripple. But the prevalent inverters are two-level inverters that are applied for low power applications and the number of voltage vectors is also low [26, 27]. Furthermore, other challenge is unbalancing of neutral point (NP) voltage in the DC3L inverters that cause harmonics in the load and high voltage stress in switching devices. In [28], balancing the voltage of the capacitors in the DC3L inverter uses an extra weighting coefficient which is challenging to adjust.

According to previous researches in field of multiphase motors control it is observed that often methods, still face challenges such as high torque ripple, heavy computational load, undesirable dynamic response and high complexity. Furthermore, the multi-phase motors are fed by two-level inverters for low powers. Hence, this paper proposes to decline the complication of MPC calculations by decreasing the number of acceptable voltage vectors that improve MPC performance in DTP-BLDCM fed by two DC3L inverters. Also, the suggested strategy focuses on reducing the torque ripple to eliminate mechanical vibration or acoustic noise that is unacceptable in sensitive medium voltage applications. The number of switching states reduces from 729 to 36 per each control cycle, which decreases computation time considerably. Since tuning the weight coefficients is challenging, a method to balance the capacitor voltage without needing a weighting coefficient is presented to eliminate a capacitor balancing objective in the cost function. The results of the suggested MPC strategy are compared and analyzed with the (MHC) multiband hysteresis current controller method through simulation.

The rest of this paper is organized as follows. Section 2 discusses the model of DTP-BLDCM and the performance of DC3L inverter. Section 3 contains the suggested MPC strategy and comparing with the MHC controller, selection of voltage vectors and the method presented for DC3L inverter capacitor voltage balancing and section 4 presents results and analysis. Finally, some conclusions are presented in section 5.

MATLAB/Simulink environment is used for simulations that evaluates the feasibility and execution of the suggested MPC strategy with the specification of 4125-V/2.7-MW/350-RPM DTP-BLDCM. The suggested MPC control approach presents lower torque ripple and

better quantitative and qualitative features in comparison to the MHC control approach and the classical MPC control.

2 System Configuration and Modeling

Multiphase motors modeling methods are divided into two groups: vector space decomposition model [29, 30] and individual multiple three-phase model. The vector space decomposition (VSD) method, the motor model is formulated by using one $\alpha\beta$ subspace, xy subspaces and zero sequence components, which cause independent current regulation in these subspaces. In this paper, the under-study motor is investigated using the individual dual three-phase model due to the advantages of modular modeling and separate control of each three-phase set [31].
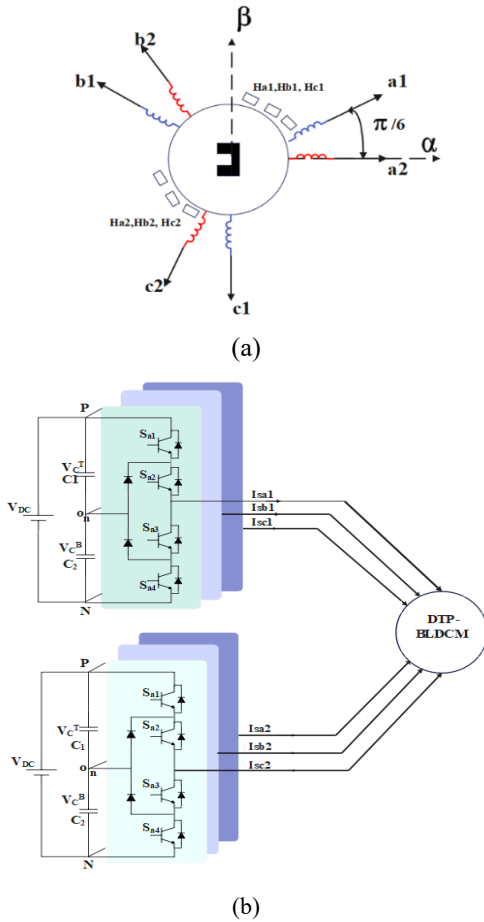

(a)

(b)

Fig 1. (a) drive system (b) DTP-BLDCM

Fig. 1(a) shows the DC3L inverters fed DTP-BLDCM including two sets of three-phase windings, which 30 electrical degrees is transferred and the neutral points of the both of sets is isolated. Fig. 1(b) represents the configuration of DTP-BLDCM.

The mutual inductance are described by Eq. (1) [32]:

$$M_{ij} = \frac{2}{3} L_m \cos(\theta_{ei} - \theta_{ej})$$
$$= \frac{2}{3} L_m \cos(\Delta\theta_{eij}) \tag{1}$$

The rotor electrical positions of stator windings are shown by θ_{ei}, θ_{ej} and L_m is magnetizing inductance. The electrical displacements one of the three-phase windings are $0, \pm 120°, \pm 240°$. Also, the electrical displacements the first and the second three-phase winding are $\pm 30°, \pm 150°, \pm 270°$, separately. The voltage vector can be can be written as below form [32]:

$$\vec{u}_s = R_s \vec{i}_s + L \frac{d\vec{i}_s}{dt} + \vec{e} \tag{2}$$

$$L_{s1} = L_{s2} = \frac{2}{3} \begin{bmatrix} \frac{3}{2}L_{ls} + L_m & -\frac{1}{2}L_m & -\frac{1}{2}L_m \\ -\frac{1}{2}L_m & \frac{3}{2}L_{ls} + L_m & -\frac{1}{2}L_m \\ -\frac{1}{2}L_m & -\frac{1}{2}L_m & \frac{3}{2}L_{ls} + L_m \end{bmatrix} \tag{3}$$

$$M_{s1} = \frac{2}{3} L_m \frac{\sqrt{3}}{2} \begin{bmatrix} 1 & -1 & 0 \\ 0 & 1 & -1 \\ -1 & 0 & 1 \end{bmatrix} \tag{4}$$

$$M_{s2} = \frac{2}{3} L_m \frac{\sqrt{3}}{2} \begin{bmatrix} 1 & 0 & -1 \\ -1 & 1 & 0 \\ 0 & -1 & 1 \end{bmatrix} \tag{5}$$

$$L = \begin{bmatrix} L_{s1} & M_{s1} \\ M_{s2} & L_{s2} \end{bmatrix} \tag{6}$$

where $\vec{u}_s$, $\vec{i}_s$ and $\vec{e}$ are six-dimensional phase voltages, currents and back-EMF voltages vectors, respectively; R_s is a six by six stator resistance diagonal matrix that describes stator resistance of windings; L is six by six stator inductance matrix and M_{s1}, M_{s2} are mutual inductances that is shown in Eq. (6). All phases have considered with same leakage inductance L_{ls}.

The electromagnetic torque T_e produced by the DTP-BLDCM is used to drive the mechanical load T_L and overcome the damping friction B and rotational inertia J during speed acceleration. This relation can be expressed as below form:

$$T_e - T_L = J\frac{d}{dt}\omega_m \quad (7)$$
$$+ B\omega_m$$

$$T_e = \sum_{x=a1b1c1a2b2c2} T_x$$

$$= \frac{e_{a1}is_{a1} + e_{b1}is_{b1} + e_{c1}is_{c1} + e_{a2}is_{a2} + e_{b2}is_{b2} + e_{c2}is_{c2}}{\omega_m} \quad (8)$$
$$= K_t(\sum_{x=a1b1c1a2b2c2} is_x) = 4K_t\,Is$$

where ω_m is the mechanical angular velocity in rad/s.

In under study DTP-BLDCM, the electromagnetic torque has direct relationship with phase current and the current flows through two phases at each set of three-phase windings for switching interval that torque can be obtained as below:

K_t is torque constant and Is is the current of the phases that conduct.

The following equation can be utilized to describe trapezoidal back-EMFs or the induced EMFs in the DTP-BLDCM:

$$e = K_e\omega_e \quad (9)$$

where K_e is the back-EMF voltage constant and ω_e is speed of DTP-BLDCM in electrical rad/s that is defined as below and p is the number of rotor poles:

$$\omega_e = \frac{p}{2}\omega_m \quad (10)$$

2.1 Modeling of DC3L Inverter

The DC3L inverter configuration is represented in Fig. 1(b). Each set of three-phase winding are fed from a separate DC3L inverter. The voltage of the DC link is V_{DC} and DC capacitors are expressed with C_1 and C_2. Each phase includes switches $S_{x1} \sim S_{x4}$ $(x = a, b, c)$ and clamping diodes. Switching states of the DC3L inverter is shown in Table 1.

There are three switching states in each phase for three-level inverters. Therefore, there are 27 switching states for the DC3L inverter corresponding to 27 voltage vectors in the space vector diagram, according to Fig. 2. Based on the amplitude, 27 voltage vectors can be classified into four types: large vectors are (V15, V17, V19, V21, V23, V25) with magnitude of $(2V_{DC}/3)$, medium vectors are (V16, V18, V20, V22, V24, V26) with magnitude of $(\sqrt{3}/3V_{DC})$, small vectors are (V3~V14) with magnitude of $(V_{DC}/3)$ and zero vectors (V0, V1, V2) [33, 34].

The neutral point voltage is written as follows:

Table 1. Switching states of the DC3L inverter

Switching state	P	O	N
S_{x1}	1	0	0
S_{x2}	1	1	0
S_{x3}	0	1	1
S_{x4}	0	0	1
Output Voltage	$V_{DC}/2$	0	$-V_{DC}/2$

$$V_n = \frac{V_C^T - V_C^B}{2} \quad (11)$$

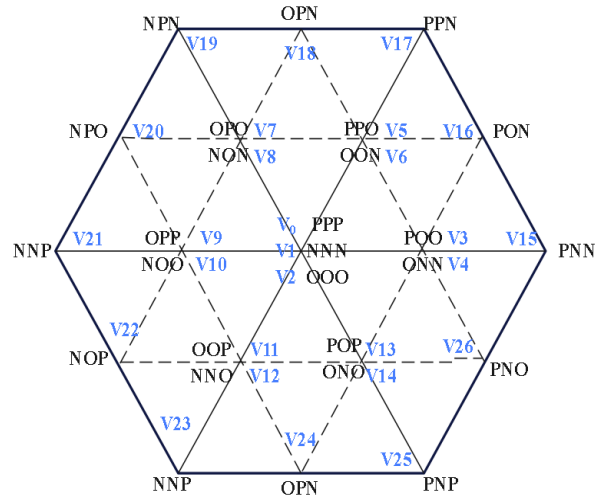V_C^T and V_C^B are the DC voltage of capacitors.

Fig 2. Diagram of space vector DC3L inverter

3 Proposed Control Strategy

For better evaluation, the multiband hysteresis current MHC controller strategy is compared with the suggested MPC controller method. DTP-BLDCM in the MHC controller similar to the suggested MPC controller are fed by two DC3L inverters. Fig. 3(a) illustrates the MHC controller scheme, briefly. The MHC controller for one phase of DC3L inverter needs two symmetrical bands. The actual current from each phase is compared with the reference current which produces an error signal. The error signal is compared by upper hysteresis controller between the up and middle band limit for the upper switches of the inverter leg. Also, the lower hysteresis controller compares the error signal between the low and middle band limit for the lower switches of the inverter leg. The signals produced from hysteresis bands are sent to Hall sensors. Switching pulses are produces based on the output of the hysteresis controllers and Hall sensors inputs. In this method, the rotor speed follows the reference speed through hysteresis bands, which makes

Table 2. States of Hall sensor, back-EMFs and Torque values

Sector	$H_{a1},H_{b1},H_{c1},H_{a2},H_{b2},H_{c2}$	$e_{a1},e_{b1},e_{c1},e_{a2},e_{b2},e_{c2}$	$T_{a1},T_{b1},T_{c1},T_{a2},T_{b2},T_{c2}$
$0 \le \theta_e < \dfrac{\pi}{3}$	0,0,1,0,0,1	0,-1,1,0,-1,1	0,1,1,0,1,1
$\dfrac{\pi}{3} \le \theta_e < \dfrac{2\pi}{3}$	1,0,1,1,0,1	1,-1,0,1,-1,0	1,1,0,1,1,0
$\dfrac{2\pi}{3} \le \theta_e < \pi$	1,0,0,1,0,0	1,0,-1,1,0,-1	1,0,1,1,0,1
$\pi \le \theta_e < \dfrac{4\pi}{3}$	1,1,0,1,1,0	1,0,-1,1,0,-1	1,0,1,1,0,1
$\dfrac{4\pi}{3} \le \theta_e < \dfrac{5\pi}{3}$	0,1,0,0,1,0	-1,1,0,-1,1,0	1,1,0,1,1,0
$\dfrac{5\pi}{3} \le \theta_e < 2\pi$	0,1,1,0,1,1	-1,0,1,-1,0,1	1,0,1,1,0,1

each phase follow its reference current. By switching frequency obtains the bandwidth of hysteresis controllers. In simulation, 2% bandwidth is chosen [34, 35].

Fig. 3(b) shows the suggested MPC controller scheme. The back-EMF values must be calculated in MPC control section.

It is used of the states of Hall sensors for obtaining back-EMFs and electromagnetic torque values according to Table 2. $H_{a1},H_{b1},H_{c1},H_{a2},H_{b2},H_{c2}$ are six Hall sensor signals. According to Eq. (8) the electromagnetic torque directly relates to the phase current. Hence, it can be specified phase which generates this electromagnetic torque value and can be found the current in which phase. So, the phase current finder block is utilized for obtaining the phase currents as shown in Fig. 3(b).

As are observed the suggested MPC control scheme contains three main parts: (1) the speed control loop that creates reference torque; (2) using of the stationary reference frame for converting of calculated back-EMFs, stator voltage and stator currents and (3) model predictive control scheme including the selection of voltage vectors, capacitor voltage balancing and formulation of the cost Function.

For MPC approach implementation, components of the back-EMFs, stator current and voltage in the αβ stationary reference frame are converted. Eq. (12) expresses the Clark transformation for both of sets windings.

The MATLAB code of the MPC block includes the turquoise blocks shown in Fig. 3(b).

$$
\begin{bmatrix} \alpha_1 \\ \beta_1 \\ \alpha_2 \\ \beta_2 \\ 0 \\ 0 \end{bmatrix} =
\begin{bmatrix}
1 & -\dfrac{1}{2} & -\dfrac{1}{2} & 0 & 0 & 0 \\
0 & -\dfrac{\sqrt{3}}{2} & \dfrac{\sqrt{3}}{2} & 0 & 0 & 0 \\
0 & 0 & 0 & \dfrac{\sqrt{3}}{2} & -\dfrac{\sqrt{3}}{2} & 0 \\
0 & 0 & 0 & \dfrac{1}{2} & \dfrac{1}{2} & 0 \\
\dfrac{1}{3} & \dfrac{1}{3} & \dfrac{1}{3} & 0 & 0 & 0 \\
0 & 0 & 0 & \dfrac{1}{3} & \dfrac{1}{3} & \dfrac{1}{3}
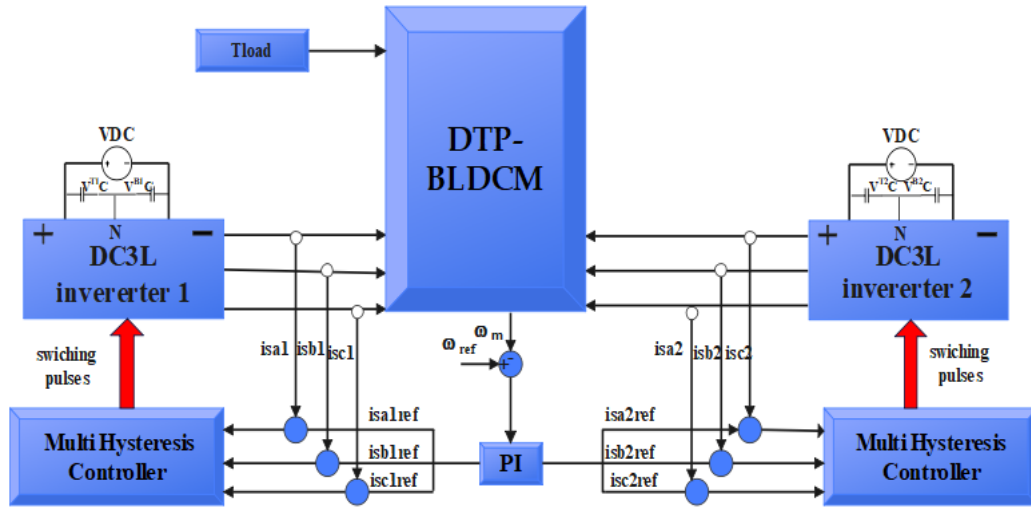\end{bmatrix}
\tag{12}
$$

Voltage equations have below form:

$$
\vec{u}_{S1,S2} = \begin{bmatrix} u_{s\alpha1} \\ u_{s\beta1} \\ u_{s\alpha2} \\ u_{s\beta2} \end{bmatrix} = R_{\alpha\beta} \begin{bmatrix} i_{s\alpha1} \\ i_{s\beta1} \\ i_{s\alpha2} \\ i_{s\beta2} \end{bmatrix} + L_{\alpha\beta} \frac{d}{dt} \begin{bmatrix} i_{s\alpha1} \\ i_{s\beta1} \\ i_{s\alpha2} \\ i_{s\beta2} \end{bmatrix} + \begin{bmatrix} e_{\alpha1} \\ e_{\beta1} \\ e_{\alpha2} \\ e_{\beta2} \end{bmatrix}
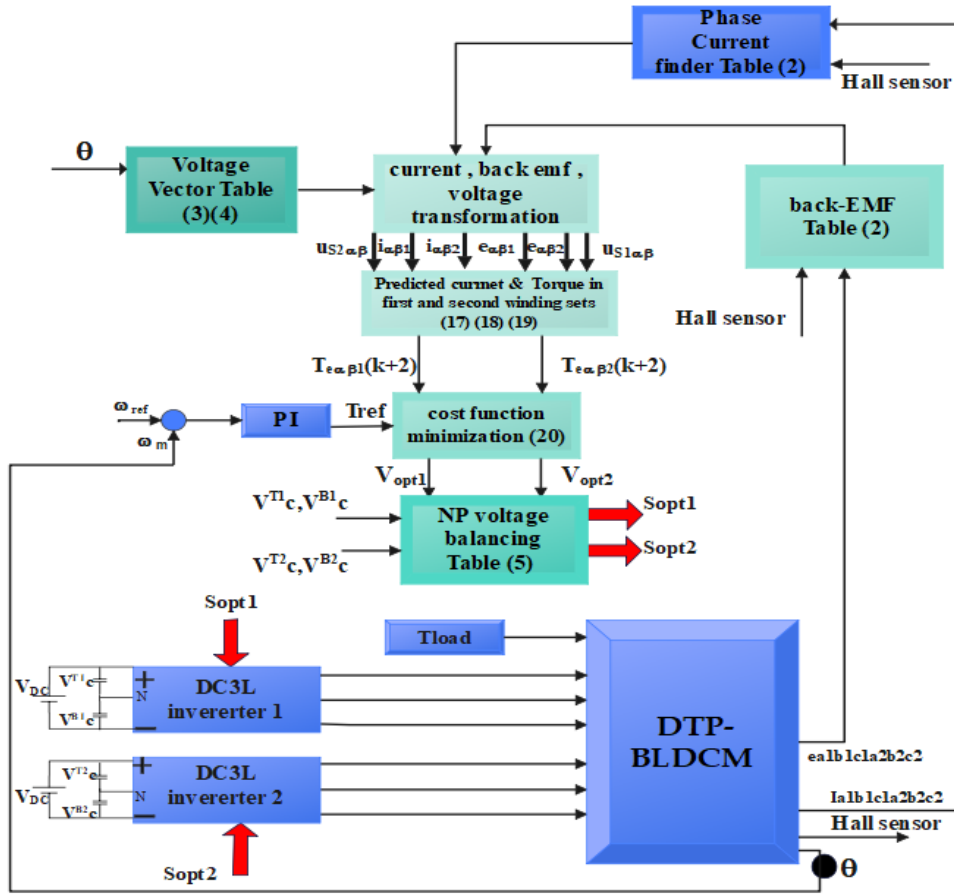\tag{13}
$$

where $L_{\alpha\beta}$ is inductance matrix in stationary reference frame that is defined as follows:

$$
L_{\alpha\beta} = \begin{bmatrix}
L_{ls}+L_m & 0 & L_m & 0 \\
0 & L_{ls}+L_m & 0 & L_m \\
L_m & 0 & L_{ls}+L_m & 0 \\
0 & L_m & 0 & L_{ls}+L_m
\end{bmatrix}
\tag{14}
$$

$R_{\alpha\beta}$ is a four by four diagonal matrix with identical stator resistance R_s. Electromagnetic torque after

(a)

(b)

Fig 3. (a) the MHC controller scheme (b) the suggested MPC scheme
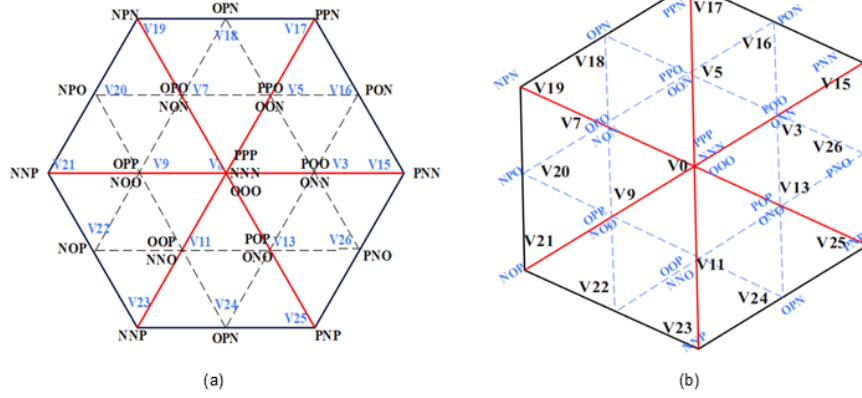
Fig 4. (a) Diagram of space vector of the first inverter (b) Diagram of space vector of the second inverter

transformation is expressed as follows:

$$T_e = \frac{2}{3}(i_{s\alpha1}e_{\alpha1} + i_{s\beta1}e_{\beta1} + i_{s\alpha2}e_{\alpha2} + i_{s\beta2}e_{\beta2})/\omega_m \qquad (15)$$

3.1 Selection of Voltage Vectors

To decrease the computational load in digital signal processor (DSP), it is essential to choose the optimal voltage vectors among the accessible vectors . In the space voltage diagram of the DC3L inverter, there are 27 voltage vectors, including 19 impressive voltage vectors and 8 redundant voltage vectors. The output voltages values of DC3L inverters are calculated by utilizing the DC link voltage and impressive switching states and then is transferred to stationary reference frame. Hence, the suggested space voltage vector diagram of two DC3L inverters is shown in Fig. 4(a) and Fig. 4(b). As can been observed, the DC3L inverter space vector diagram is divided into six equal sections. The vector diagram of the second inverter is shifted 30 degrees. The choice of the optimal voltage vector is based on the electrical position of the motor θ_e. For example, for $0 \le \theta_{e1} < \pi/3$ in the first inverter, the voltage vectors $V_0, V_3, V_5, V_{15}, V_{16}, V_{17}$ is selected and for $\pi/6 \le \theta_{e2} < \pi/2$ in the second inverter, the voltage vectors $V_0, V_3, V_{13}, V_{15}, V_{25}, V_{26}$ is selected. θ_{e1} is electrical position of the motor in first inverter and $\theta_{e2} = \theta_{e1} + \pi/6$ is the electrical position of the motor in second inverter. Table 3 and Table 4 shows optimal voltage vectors for each sector in first and second inverter, respectively. Hence, the number of switching states in each sector of the first inverter is six and in each sector of the second inverter is also six. In total, 36 switching states are checked in each control cycle, which significantly decreases the calculation time in comparison to the state where all

switching states are considered in two inverters.

Table 3. Optimal voltage vector for each θ_{e1} sector in the first inverter

Sector	Optimal voltage vector of first inverter
$0 \le \theta_{e1} < \dfrac{\pi}{3}$	$V_0, V_3, V_5, V_{15}, V_{16}, V_{17}$
$\dfrac{\pi}{3} \le \theta_{e1} < \dfrac{2\pi}{3}$	$V_0, V_5, V_7, V_{17}, V_{18}, V_{19}$
$\dfrac{2\pi}{3} \le \theta_{e1} < \pi$	$V_0, V_7, V_9, V_{19}, V_{20}, V_{21}$
$\pi \le \theta_{e1} < \dfrac{4\pi}{3}$	$V_0, V_9, V_{11}, V_{21}, V_{22}, V_{23}$
$\dfrac{4\pi}{3} \le \theta_{e1} < \dfrac{5\pi}{3}$	$V_0, V_{11}, V_{13}, V_{23}, V_{24}, V_{25}$
$\dfrac{5\pi}{3} \le \theta_{e1} < 2\pi$	$V_0, V_3, V_{13}, V_{15}, V_{25}, V_{26}$

Table 4. Optimal voltage vector for each θ_{e2} sector in the second inverter

Sector	Optimal voltage vector of second inverter
$\dfrac{\pi}{6} \le \theta_{e2} < \dfrac{\pi}{2}$	$V_0, V_3, V_{13}, V_{15}, V_{25}, V_{26}$
$\dfrac{\pi}{2} \le \theta_{e2} < \dfrac{5\pi}{6}$	$V_0, V_3, V_5, V_{15}, V_{16}, V_{17}$
$\dfrac{5\pi}{6} \le \theta_{e2} < \dfrac{7\pi}{6}$	$V_0, V_5, V_7, V_{17}, V_{18}, V_{17}$
$\dfrac{7\pi}{6} \le \theta_{e2} < \dfrac{9\pi}{6}$	$V_0, V_7, V_9, V_{19}, V_{20}, V_{21}$
$\dfrac{9\pi}{6} \le \theta_{e2} < \dfrac{11\pi}{6}$	$V_0, V_9, V_{11}, V_{21}, V_{22}, V_{23}$
$\dfrac{11\pi}{6} \le \theta_{e2} < \dfrac{\pi}{6}$	$V_0, V_{11}, V_{13}, V_{23}, V_{24}, V_{25}$

A. Computational Burden Investigation

The dSPACE Profiler is used to measure the execution times of the MPC scheme with (19×19=361) impressive voltage vectors (the classical MPC) and the suggested MPC scheme with 36 voltage vectors and are compared in Fig. 15 in detail. As can be observed the classical MPC scheme occupies the high computational. The optimization process with the optimal voltage vectors occupies 22μs where the lower computational amount is obtained in comparison to classical MPC scheme. The time of the suggested MPC controller is completed within the sampling interval 50μs. As can be observed the execution time estimation block occupies the largest computational burden since the updating matrices calculation. The process the classical MPC occupies 42.5μs. As a result, computational time up to 1.48 times reduces in the suggested MPC scheme than the classical MPC.
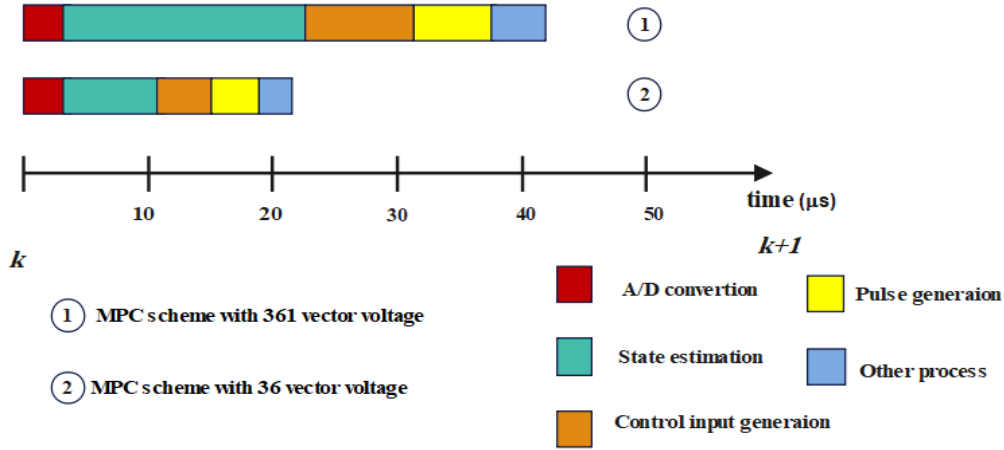
3.2 Capacitors Voltage Balancing

Unbalanced DC-link capacitor voltages cause current distortion, damage capacitors and increase torque ripple. Therefore, the neutral point (NP) voltage should be around zero volts. For example, the small positive vector OPO increases the midpoint voltage and the small negative vector NON decreases the midpoint voltage [36, 37].

In this paper, small opposite vectors are chosen from the voltage vector diagram according to Table 5 that balance DC link capacitor voltages without weighting coefficients for the cost function. Hence, the control complication reduces due to lack of need to adjustment weighting coefficient. Therefore, the cost function in the suggested MPC method don't apply the NP voltage objective function similar to some references that have used the weighting coefficients [38].

Fig 5. The execution time of the classical MPC scheme and the suggested MPC scheme

Table 5. Optimal small vector for capacitor voltage balancing of first and second inverter

$V_{Optimal}$	$V_{C1}^{T} \geq V_{C1}^{B}$	$V_{C1}^{T} < V_{C1}^{B}$	$V_{C2}^{T} \geq V_{C2}^{B}$	$V_{C2}^{T} < V_{C2}^{B}$
V_{3}	POO	ONN	POO	ONN
V_{5}	PPO	OON	PPO	OON
V_{7}	OPO	NON	OPO	NON
V_{9}	OPP	NOO	OPP	NOO
V_{11}	OOP	NNO	OOP	NNO
V_{13}	POP	ONO	POP	ONO

3.3 Formulation of the Cost Function

For suggested MPC control implementation, the Euler approximation could be used as:

$$\frac{dx}{dt} = \frac{x(k+1) - x(k)}{T_s} \qquad (16)$$

where x is the control variable and T_s is the sampling time. The MPC technique uses the discrete equations of the system and derives the discrete model. By applying this approximation to Eq. (13), the Eq. (17) can be achieved which indicates future values of current in next sampling interval. Hence, the subsequent status of the system is predicted by the calculation of the next sampling time and by minimizing the cost function that specifies the optimal switching modes.

$$\begin{bmatrix} i_{s\alpha1}(k+1) \\ i_{s\beta1}(k+1) \\ i_{s\alpha2}(k+1) \\ i_{s\beta2}(k+1) \end{bmatrix} = \frac{T_s}{L_{\alpha\beta}} \left(\begin{bmatrix} u_{s\alpha1}(k) \\ u_{s\beta1}(k) \\ u_{s\alpha2}(k) \\ u_{s\beta2}(k) \end{bmatrix} - \begin{bmatrix} e_{\alpha1}(k) \\ e_{\beta1}(k) \\ e_{\alpha2}(k) \\ e_{\beta2}(k) \end{bmatrix} - R_{\alpha\beta} \begin{bmatrix} i_{s\alpha1}(k) \\ i_{s\beta1}(k) \\ i_{s\alpha2}(k) \\ i_{s\beta2}(k) \end{bmatrix} \right) + \begin{bmatrix} i_{s\alpha1}(k) \\ i_{s\beta1}(k) \\ i_{s\alpha2}(k) \\ i_{s\beta2}(k) \end{bmatrix} \quad (17)$$

It should be noted that half of the torque is provided by the first stator windings set and other half of the torque is provided by the second stator windings set. The predicted torque of the first and second stator windings set is described separately based on the predicted current is expressed with the following equations:

$$T_{e\alpha\beta1}(k+1) = \frac{3}{2}(i_{s\alpha1}(k+1)e_{\alpha1}(k) + i_{S\beta1}(k+1)e_{\beta1}(k))/\omega_m \quad (18)$$

$$T_{e\alpha\beta2}(k+1) = \frac{3}{2}(i_{s\alpha2}(k+1)e_{\alpha2}(k) + i_{S\beta2}(k+1)e_{\beta2}(k))/\omega_m \quad (19)$$

The reference torque is produced by a PI controller. The suggested MPC controller aims to follow $T_{e\alpha\beta}(k+1)$ the reference torque. The suggested MPC scheme obtains the predicted torque utilizing Eq. (13)-Eq. (19). The predicted and reference torque values of the first and the second stator windings set are compared in a cost function. All 36 switching states are investigated and the state that minimizes the cost function as the next switching mode is exerted to the two DC3L inverters. To lessen the computational burden, the delay compensation technique is used. This strategy computes the predicted values in the shifted forward next sample value [39]. Consequently, cost function of the suggested MPC strategy is expressed as follows:

$$g = (0.5T_{eref} - T_{e\alpha\beta1}(k+2))^2 + (0.5T_{eref} - T_{e\alpha\beta2}(k+2))^2 \quad (20)$$

4 Results And Analysis

To simulate, MATLAB/Simulink is utilized to evaluate the suggested MPC control of DTP-BLDCM Fed by two DC3L inverters. The DTP-BLDCM model used in the simulation is according to section 2. The system specifications is represented in Table 6. To create DC link voltage with minimal ripple at the input of the inverters, a 24-pulse rectifier, including four 6-pulse rectifiers, is used results DC voltage of 4125 V. The speed waveforms of the MHC control and the suggested MPC strategy under constant torque are shown in Fig 6(a) and Fig 6(b). At t=0 s, reference speed is 150 rpm and changes to 350 rpm at t=0.2 s. As can be observed, the real speed of the motor tracks the command speed well in both of control schemes. Also, zoomed the Fig. 6(c) and Fig. 6(d) shows that actual and the reference speed error is 1.14% in the MHC controller, while, this error is less than 1% in the suggested MPC scheme and the speed tracking precision is high. The MHC controller is highly dependent the switching frequency. However, the suggested MPC strategy modifies the control loop at

medium sampling frequencies. For example, if the MHC controller works with the 40kHz sampling frequency, it shows better execution than with the 20kHz sampling frequency. However, in this simulation, the suggested MPC strategy operates with 20kHz switching frequency well. Hence, the MPC strategy has fewer switching losses than the MHC controller due to the switching frequency reduction. Therefore, the suggested MPC strategy has higher efficiency.

Table 6. Parameters of DTP-BLDCM

Parameter	Value
DC-link voltage V_{DC} (V)	4125
Rated Speed (rpm)	350
Power rating (MW)	2.7
Rated torque (N.m)	73000
number of poles (p)	20
Phase Resistance R_s (mΩ)	5.6
Phase Inductance L_m (mH)	265
Mutual Inductance (mH)	110
Inertia constant (Kg.m^2)	60
Back-EMF constant (V/rpm)	0.923
Sampling interval (μs)	50
Capacitor (F)	10

To investigate the waveforms in the time interval of 0 to 0.5 s, reference speed of 250 rpm is applied to the DTP-BLDCM drive and the rotor direction is reversed from 250 rpm to -250 rpm in t=0.2 s with using speed command. At the start, the DTP-BLDCM drive works in no load mode and a constant load torque 73000 (N.m) is exerted to the system at t=0.15 s. Fig. 7 and Fig. 10 show the speed waveform, electromagnetic torque waveform and current one of phases of the suggested MPC controller and the MHC controller, respectively. As can be seen, both two control schemes present acceptable tracking performance of reference speed and acceptable tracking of full load torque in motoring and braking conditions. Fig. 8 and Fig. 11 show the electromagnetic torque ripple with zoom in the suggested MPC controller and MHC controller in bidirectional mode. The torque ripples of the MHC controller and the suggested MPC controller in motoring mode is 10000 N.m and 19000 N.m, respectively and the torque ripples of the MHC controller and the suggested MPC controller in reverse mode are 20000 N.m and 7000 N.m, respectively. Thus, the suggested MPC controller reduces the electromagnetic torque ripple 47.6% in motoring mode and 64.8% in reverse mode. Also, electromagnetic torque in the suggested MPC controller scheme in comparison to the MHC controller scheme is smoother. Moreover, Fig. 9 and Fig. 12 represents that the suggested MPC controller has a lower current ripple in comparison to the MHC controller. The current ripples

of the MHC controller and the suggested MPC controller in motoring mode is 10000 and 19000 A, respectively and the current ripples of the MHC controller and the suggested MPC controller in reverse mode are 20000 A and 7000 A, respectively. Thus, the suggested MPC controller reduces the current ripple 62.5% in motoring mode and 11% in reverse mode. Another advantage that suggested MPC controller has over the MHC controller is that to decrease the torque response time. To evaluate this test, the amount of torque decreases from full load 73000 N.m to 29200 N.m and the torque response time reduces from 120 μs to 100 μs, as represented in Fig. 13(a) and Fig. 13(b). Moreover, in the suggested MPC controller, the torque response in this interval of time is fast and smooth while, is slow and uneven in the MHC controller.

Fig. 14 shows the electromagnetic torque response in unbalancing mode of capacitors voltage that provides higher electromagnetic torque ripple than balancing mode of capacitors voltage. The torque ripples with and without balancing of capacitors voltage in motoring mode is 11000 and 29000 N.m, respectively. Table 7 compares two control methods quantitatively and qualitatively. Fig. 15(a), Fig. 15(b), Fig. 15(c) and Fig. 15(d) show the DC link capacitor voltage waveforms in suggested MPC controller with scheme applied of balancing the DC link capacitor voltages described in 3.2. As can be seen, difference between the up and low capacitor voltages in balancing mode has a small error. In contrast, up and low capacitor voltages in unbalancing mode have significant error. Fig 16 shows the speed waveform, electromagnetic torque waveform and current

one of phases of the classical MPC controller that increases the electromagnetic torque and current ripple than the suggested MPC controller. As can be seen in Table 7, the efficiency in the suggested MPC controller increases by 33% due to the reduction of torque ripple.

4.1 Sensitivity analysis

Uncertainty of some of the system parameters has a considerable effect on the efficiency of MPC strategy and puts a system's stability at risk. This problem arises because the FCS-MPC method requires system model. Uncertainty of parameters in the control method can be various, the most crucial inexactitude in parameters of the motor model. The stability of the suggested MPC controller versus to R_s, L_m and load torque T_L are investigated this section. The speed error and the torque ripple variations due to, the changes in R_s and L_m are shown in Fig. 17(a) and Fig. 17(b). According to figures, torque ripple is significantly affected by changes of R_s and L_m. R_s in Eq. (17) is coefficient of T_s. Therefore, small values of R_s doesn't have a considerable effect on the results while, torque ripple increases with higher values of R_s due to future estimates present incorrect results. When R_s values increase, the torque ripple increases due to wrong future estimates. So, the predicted MPC controller is able to tolerate changes in stator winding resistance. Fig. 17(c) shows the variation effect of load torque on speed and torque at loads less than the rated load and is acceptable.
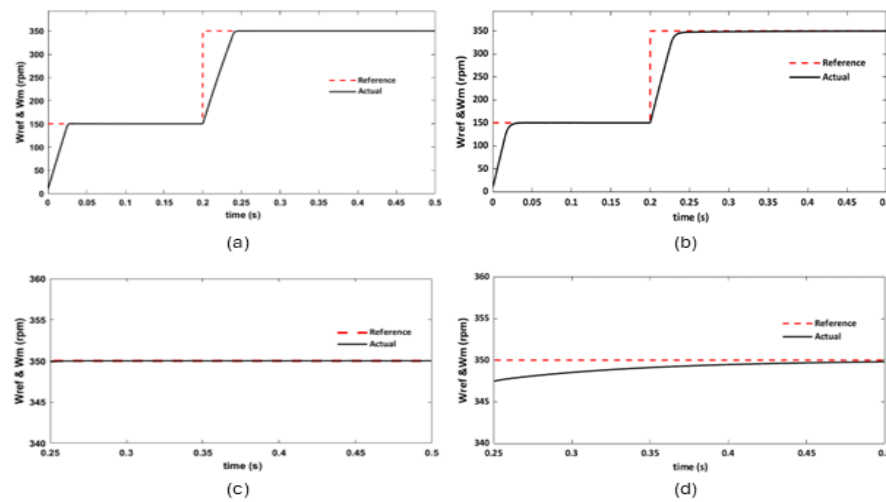

Fig 6. Speed waveform of DTP-BLDCM under rated constant torque (a) suggested MPC controller, (b) MHC strategy (c) with zoom, (d) with zoom.
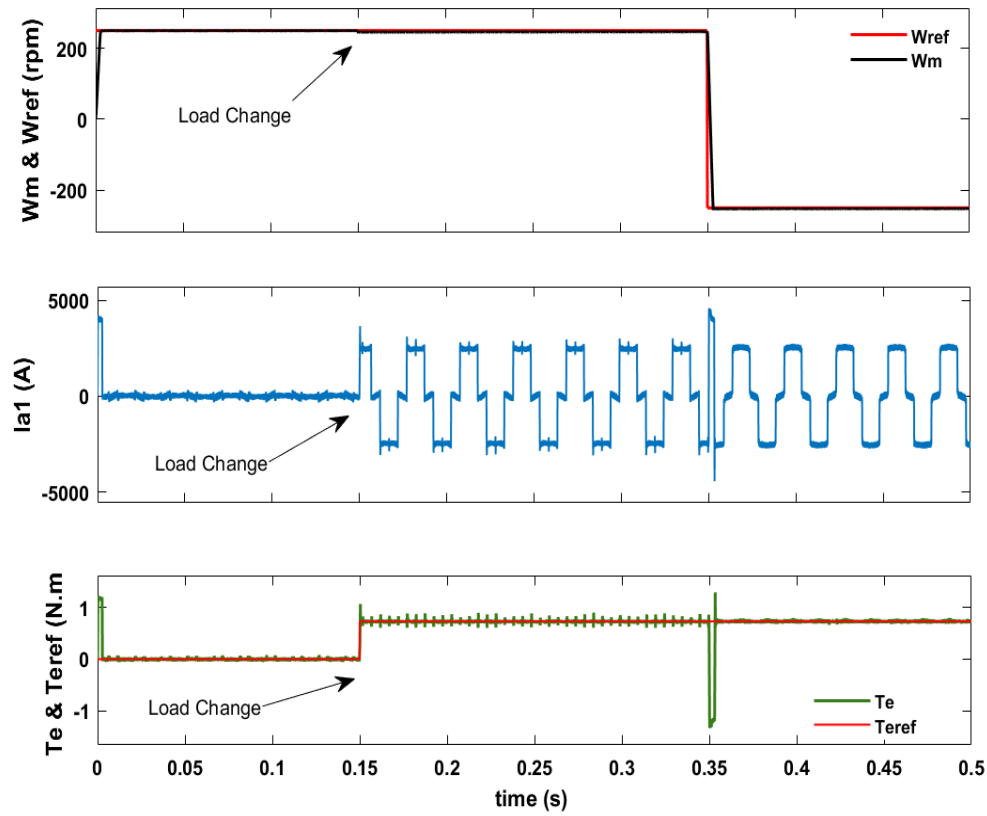
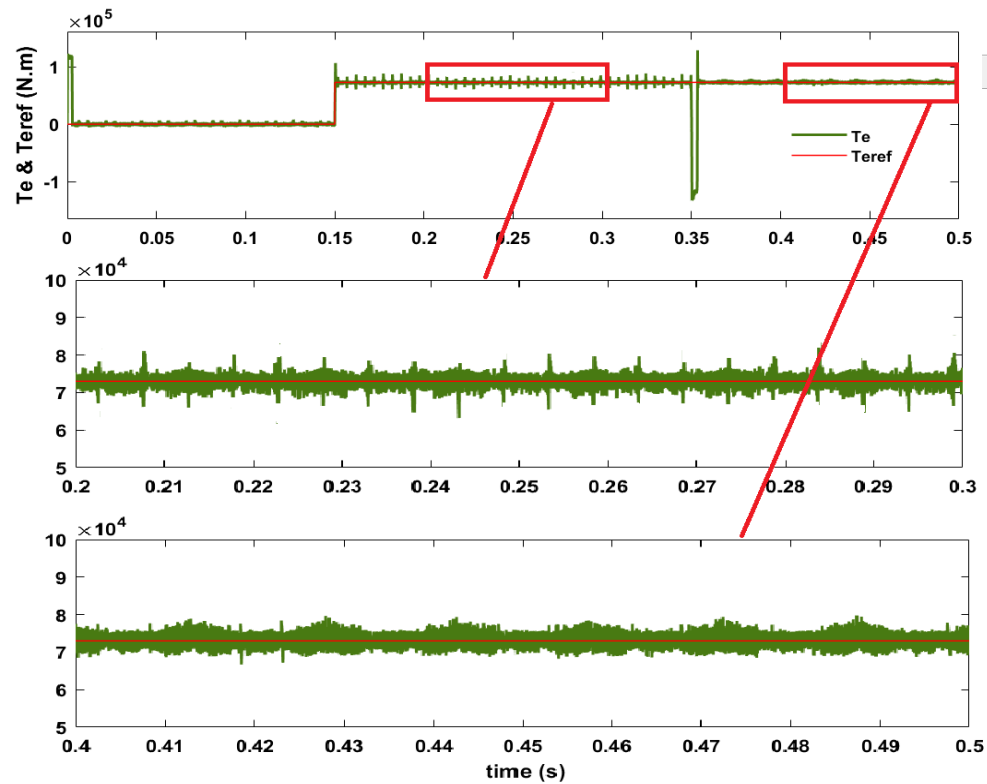**Fig 7.** Speed, electromagnetic torque and phase current waveforms with suggested MPC controller

Fig 8. Electromagnetic torque ripple with suggested MPC controller with zoom-in motoring and braking modes
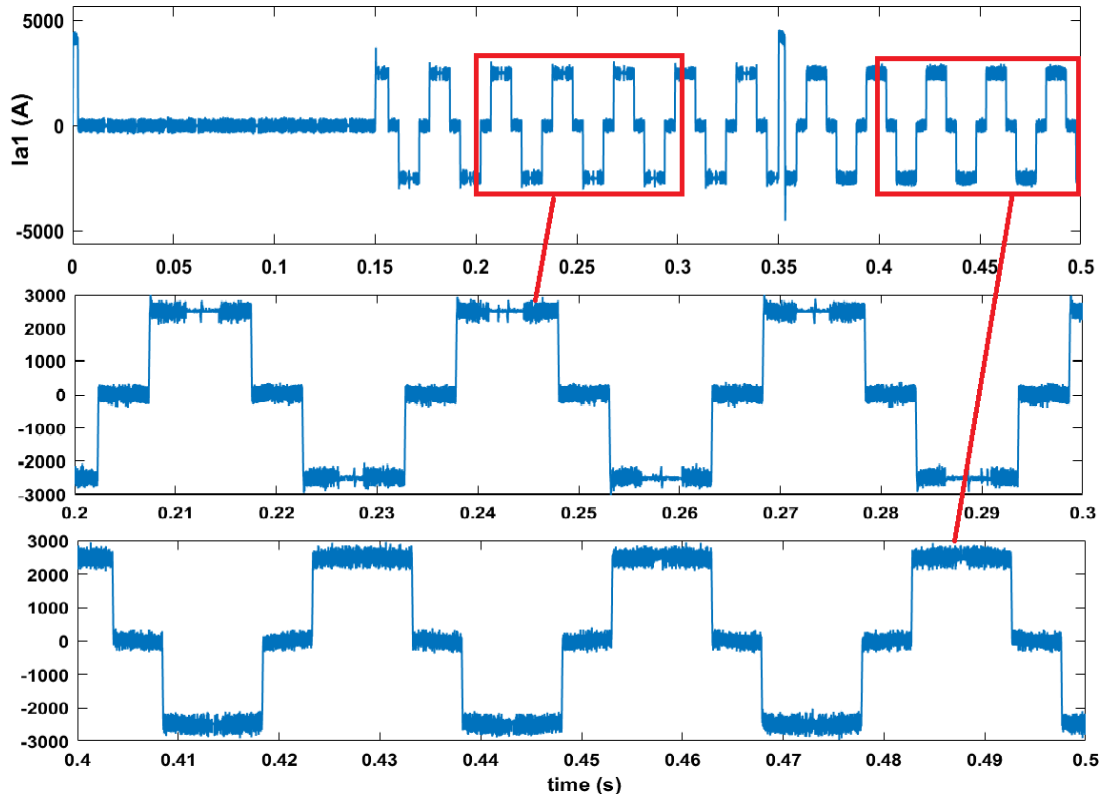
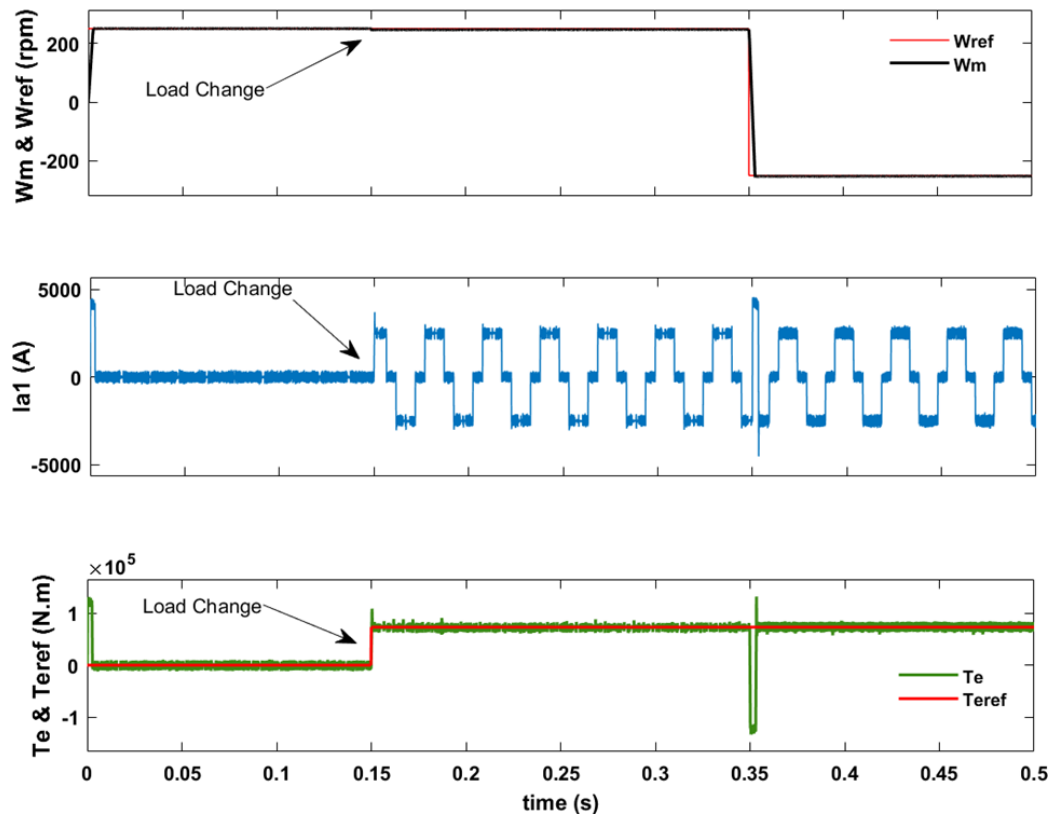**Fig 9.** Current ripple with MHC controller with zoom-in motoring and braking modes

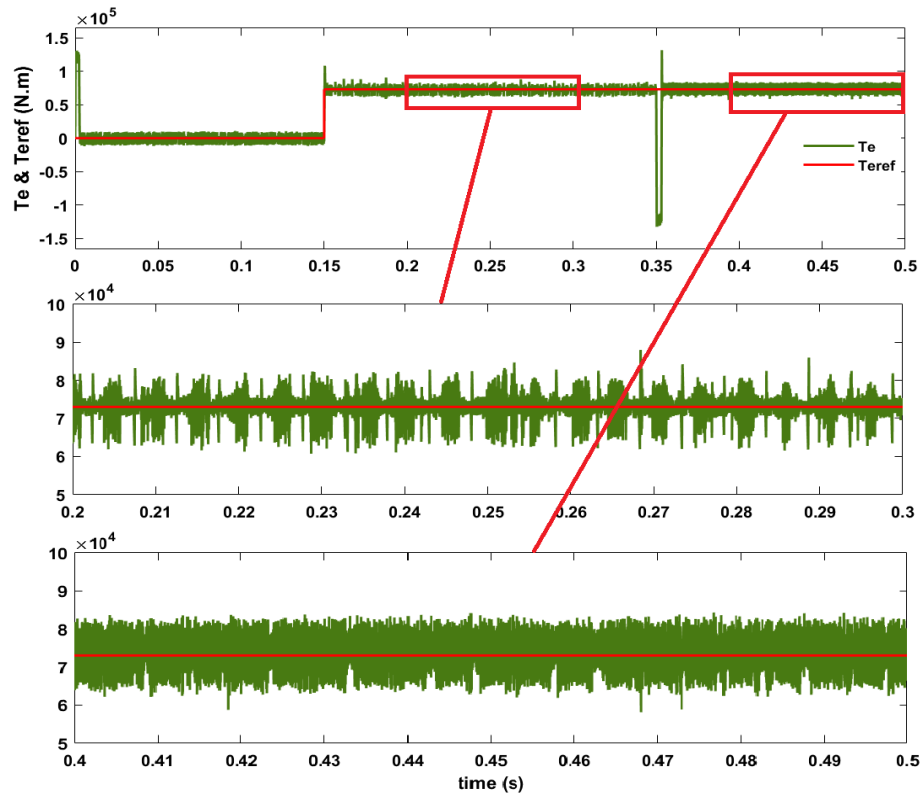**Fig 10.** Speed, electromagnetic torque and phase current waveforms with MHC controller

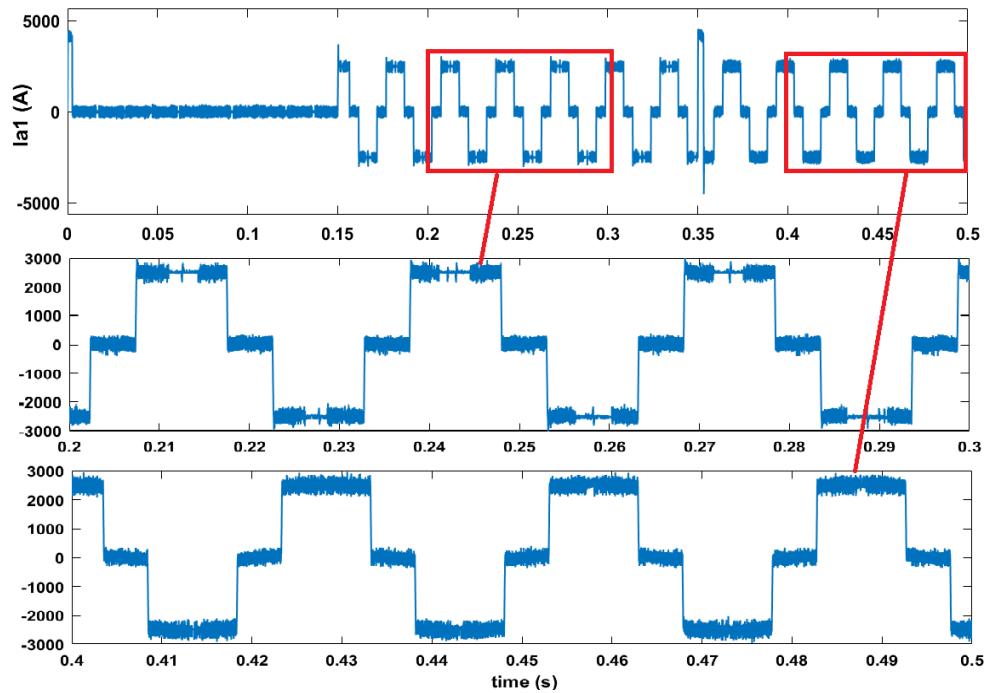**Fig 11.** Electromagnetic torque ripple with MHC controller with zoom-in motoring and braking modes

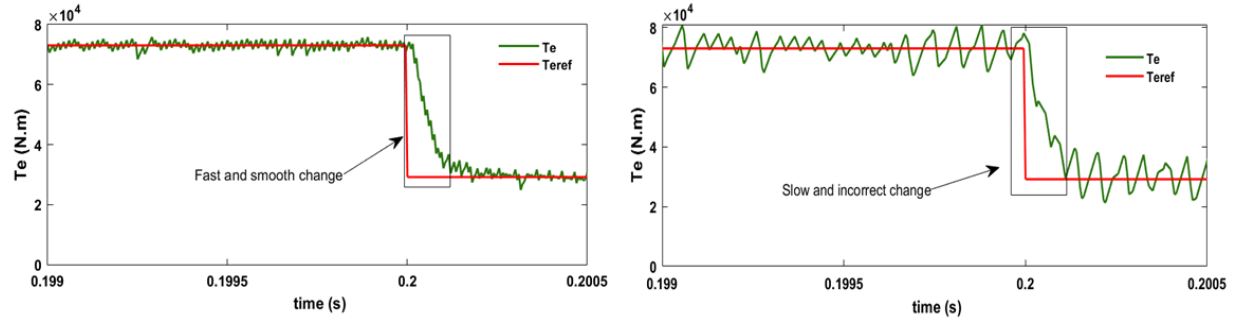**Fig 12.** Current ripple with MHC controller with zoom-in motoring and braking modes

Fig 13. Zoom of the electromagnetic torque response in rated speed: (a) suggested MPC controller (b) MHC controller
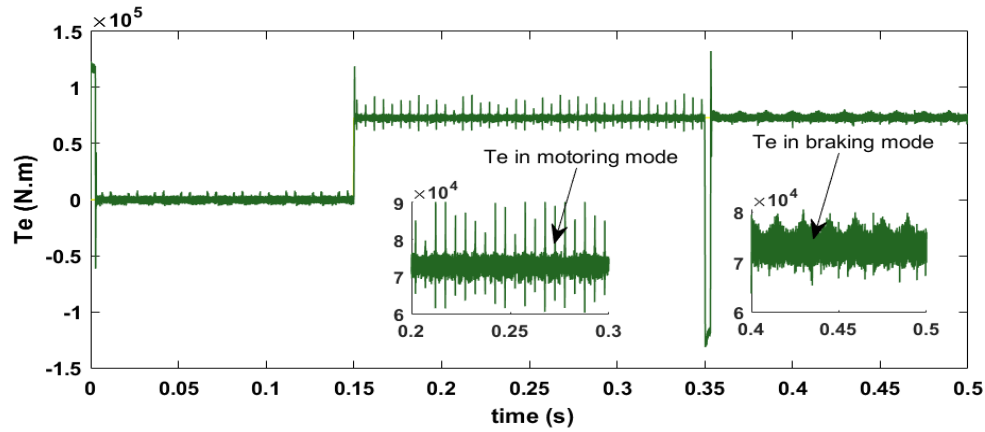

Fig 14. The electromagnetic torque response in unbalancing mode with zoom-in motoring and braking modes
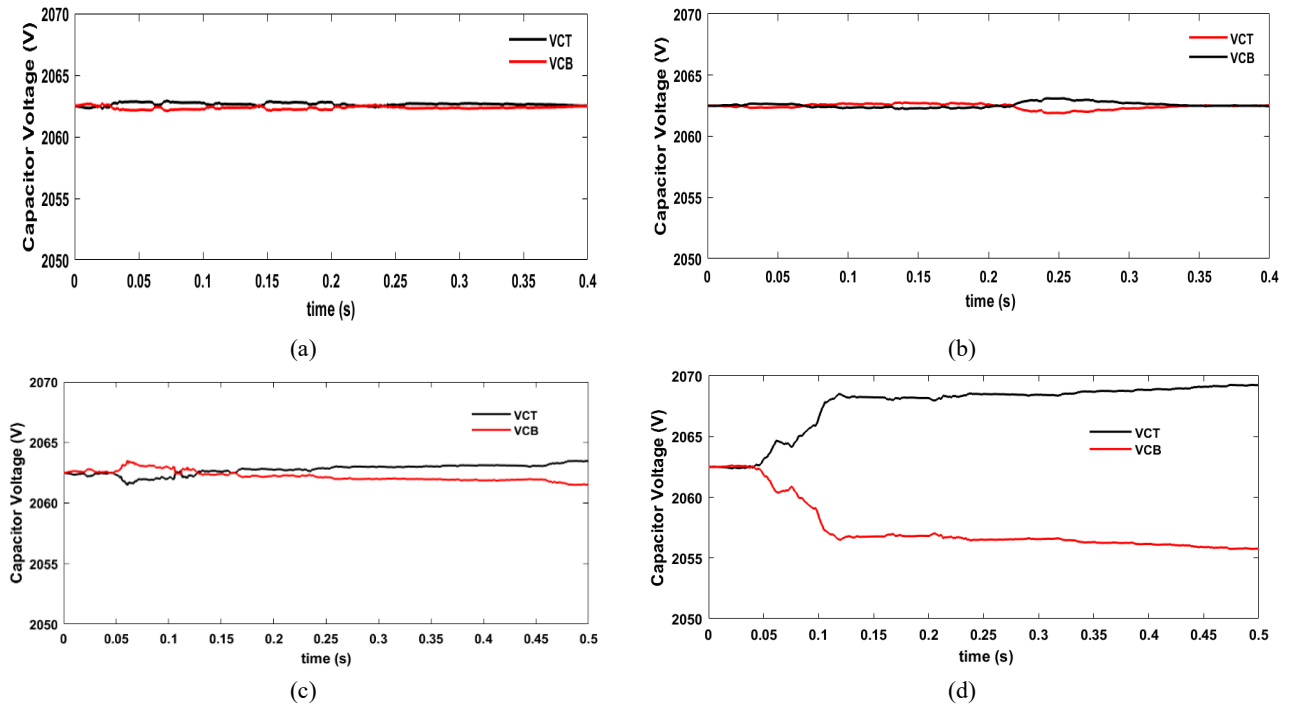

(a)

(b)

(c)

(d)

Fig 15. DC-link capacitor voltages waveforms in suggested MPC controller with rated constant speed and torque in balancing and unbalancing modes a) balanced capacitor voltages of first DC3L inverter b) balanced capacitor voltages of second DC3L inverter c) unbalanced capacitor voltages of first DC3L inverter d) unbalanced capacitor voltages of second DC3L inverter
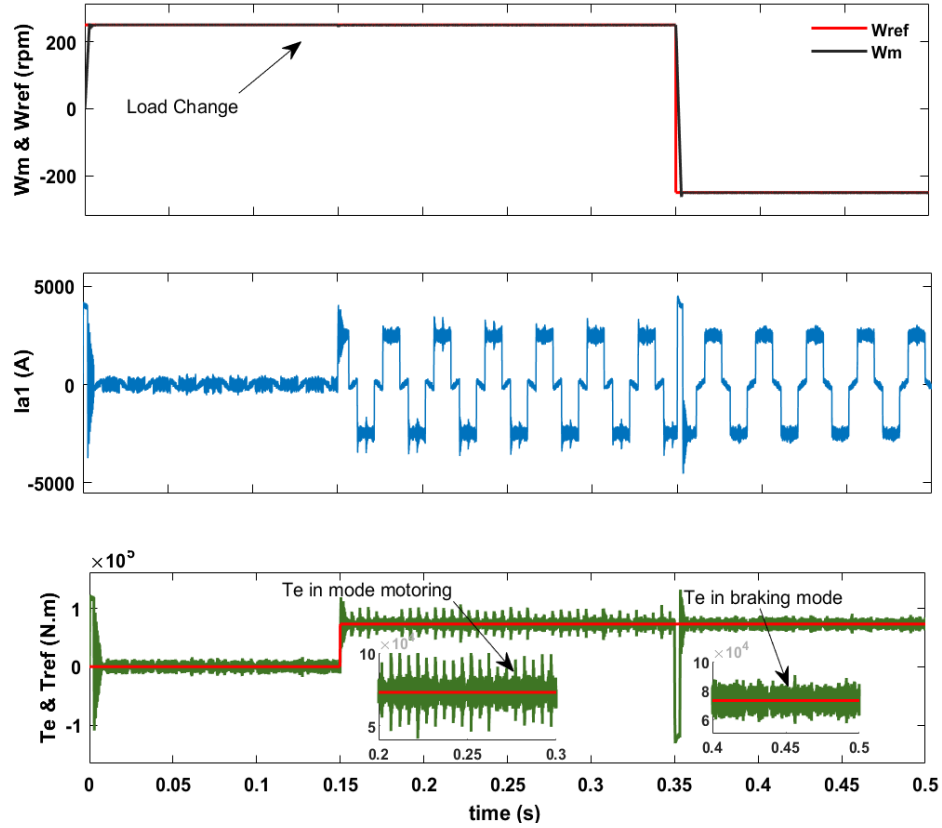
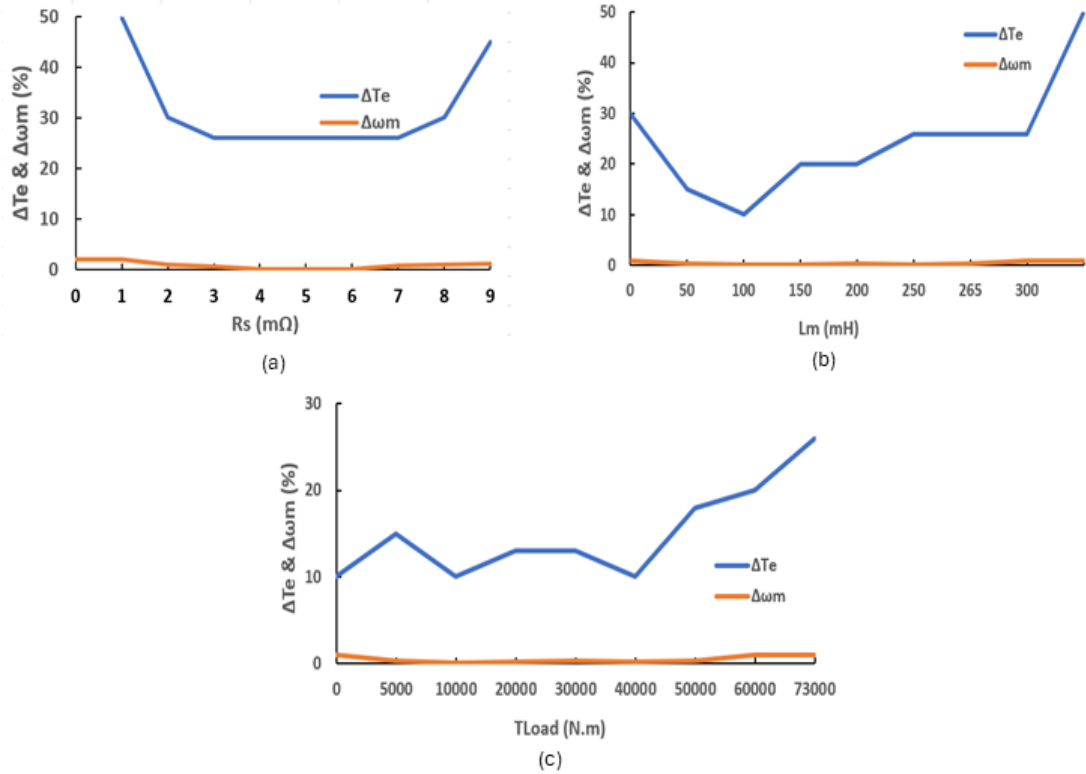**Fig 16.** Speed, electromagnetic torque and phase current waveforms with classical MPC controller

Fig 17. Sensitivity analysis: a) the variation effect of stator resistance on speed and torque, b) the variation effect of stator inductance on speed and torque c) the variation effect of load torque on speed and torque

Table 7. Quantitative and qualitative comparison of two control strategy

Parameter	Methods		
	MHC	Suggested MPC	Classical MPC
Speed tracking	Low	High	Medium
Speed error	1.42%	<1%	1%
$\Delta T_e (N.m)$ $\quad \omega_{ref} = 250 rpm$	19000	10000	
$\Delta T_e (N.m)$ $\quad \omega_{ref} = -250 rpm$	20000	7000	
$\Delta T_{e\,max} / T_e$ $\quad \omega_{ref} = 250 rpm$	26%	13.6%	54.7%
$\Delta T_{e\,max} / T_e$ $\quad \omega_{ref} = -250 rpm$	27%	9.5%	27%
$\Delta T_e (N.m)$ $\quad \omega_{ref} = 250 rpm$ without capacitor balancing		29000	
$\Delta T_e (N.m)$ $\quad \omega_{ref} = 250 rpm$ with capacitor balancing		11000	40000
$\Delta T_{e\,max} / T_e$ $\quad \omega_{ref} = 250 rpm$ without capacitor balancing		39.7%	
$\Delta T_{e\,max} / T_e$ $\quad \omega_{ref} = -250 rpm$ with capacitor balancing		15.1%	20000
Torque smoothness	Poor	High	medium
$\Delta Is (A)$ $\quad \omega_{ref} = 250 rpm$	800	300	900
$\Delta Is (A)$ $\quad \omega_{ref} = -250 rpm$	900	800	700
$\Delta Is_{max} / Is$ $\quad \omega_{ref} = 250 rpm$	32%	12%	36%
$\Delta Is_{max} / Is$ $\quad \omega_{ref} = -250 rpm$	36%	32%	28%
Response time to reference torque changing(μs)	120	100	
Computational time		22μs	42.5μs

5 Conclusion

This paper has suggested an optimized MPC control strategy to reduce torque ripple of the DTP-BLDCM drive fed by two the DC3L inverters for the application of medium voltage which are sensitive to noise and ripple. The torque and current ripple of suggested MPC control compared to the MHC control, improves both in motoring and reverse modes. In addition, the proposed MPC controller enables the actual speed to track the motor reference speed with high accuracy. The suggested MPC method by selecting the voltage vectors from both inverters has reduced the optimal switching states in each control cycle. Thus, the complexity of the computations has been reduced. The voltage balancing of the capacitors in both the DC3L inverters was simply done without of need a weighting coefficient. The electromagnetic torque ripple in balancing mode of capacitors voltage is lower than unbalancing mode of capacitors voltage in the suggested MPC controller. The simulation results prove the advantages of the suggested MPC against the classical MPC controller and the MHC controller, which are expressed as follows:

- Reduction of computational time up to 1.48 times than the classical MPC scheme;
- Faster smoother dynamic response of the suggested MPC controller than the MHC controller;
- Lower torque ripple up to 47.6% the suggested MPC controller than the MHC controller;
- Lower torque ripple up to 33% the suggested MPC controller than the classical MPC controller;

Conflict of Interest

The authors declare no potential conflict of interest regarding the publication of this work. In addition, the ethical issues including plagiarism, informed consent, misconduct, data fabrication and, or falsification, double publication and, or submission, and redundancy have been completely witnessed by the authors.

References

[1] F. Barrero and M. J. Duran, "Recent advances in the design, modeling, and control of multiphase machines—Part I," *IEEE Transactions on Industrial*

Electronics, vol. 63, no. 1, pp. 449-458, Januray 2015.

[2] E. Levi, "Multiphase electric machines for variable-speed applications," *IEEE Transactions on industrial electronics,* vol. 55, no. 5, pp. 1893-1909, May 2008.

[3] M. Mengoni, L. Zarri, A. Tani, L. Parsa, G. Serra, and D. Casadei, "High-torque-density control of multiphase induction motor drives operating over a wide speed range," *IEEE Transactions on Industrial Electronics,* vol. 62, no. 2, pp. 814-825, July 2014.

[4] P. Bogusz, M. Korkosz, and J. Prokop, "A study of dual-channel brushless DC motor with permanent magnets," in *2016 13th Selected Issues of Electrical Engineering and Electronics (WZEE)*, May 2016: IEEE, pp. 1-6.

[5] Z. Fu, J. Liu, and Z. Xing, "Performance analysis of dual-redundancy brushless DC motor," *Energy Reports,* vol. 6, pp. 829-833, December 2020.

[6] I. Shchur and V. Turkovskyi, "Open-end winding dual three-phase BLDC motor drive system with integrated hybrid battery-supercapacitor energy storage for electric vehicle," in *2021 IEEE International Conference on Modern Electrical and Energy Systems (MEES)*, September 2021: IEEE, pp. 1-6.

[7] Z. Zhu, S. Wang, B. Shao, L. Yan, P. Xu, and Y. Ren, "Advances in dual-three-phase permanent magnet synchronous machines and control techniques," *Energies,* vol. 14, no. 22, p. 7508, Novamber 2021.

[8] Y. Ren, Z. Zhu, J. E. Green, Y. Li, S. Zhu, and Z. Li, "Improved duty-ratio-based direct torque control for dual three-phase permanent magnet synchronous machine drives," *IEEE Transactions on Industry Applications,* vol. 55, no. 6, pp. 5843-5853, December 2019.

[9] Y. Hu, Z.-Q. Zhu, and K. Liu, "Current control for dual three-phase permanent magnet synchronous motors accounting for current unbalance and harmonics," *IEEE Journal of Emerging Selected Topics in Power Electronics,* vol. 2, no. 2, pp. 272-284, June 2014.

[10] A. Dey, P. Rajeevan, R. Ramchand, K. Mathew, and K. Gopakumar, "A space-vector-based hysteresis current controller for a general n-level inverter-fed drive with nearly constant switching frequency control," *IEEE Transactions on Industrial Electronics,* vol. 60, no. 5, pp. 1989-1998, May 2012.

[11] K.-H. Kim and M.-J. Youn, "DSP-based high-speed sensorless control for a brushless DC motor using a DC link voltage control," *Electric Power Components Systems,* vol. 30, no. 9, pp. 889-906, November 2002.

[12] B.-K. Lee and M. Ehsani, "Advanced simulation model for brushless dc motor drives," *Electric power components systems,* vol. 31, no. 9, pp. 841-868, June 2003.

[13] F. Barrero, M. R. Arahal, R. Gregor, S. Toral, and M. J. Durán, "A proof of concept study of predictive current control for VSI-driven asymmetrical dual three-phase AC machines," *IEEE Transactions on Industrial Electronics,* vol. 56, no. 6, pp. 1937-1954, June 2009.

[14] B. Cao, B. M. Grainger, X. Wang, Y. Zou, G. F. Reed, and Z.-H. Mao, "Direct torque model predictive control of a five-phase permanent magnet synchronous motor," *IEEE Transactions on Power Electronics,* vol. 36, no. 2, pp. 2346-2360, February 2020.

[15] W. Xie *et al.*, "Finite-control-set model predictive torque control with a deadbeat solution for PMSM drives," *IEEE Transactions on Industrial Electronics,* vol. 62, no. 9, pp. 5402-5410, September 2015.

[16] Y. Zhang, B. Zhang, H. Yang, M. Norambuena, and J. Rodriguez, "Generalized sequential model predictive control of IM drives with field-weakening ability," *IEEE Transactions on Power Electronics,* vol. 34, no. 9, pp. 8944-8955, September 2018.

[17] J. J. Aciego, I. G. Prieto, and M. J. Duran, "Model predictive control of six-phase induction motor drives using two virtual voltage vectors," *IEEE Journal of Emerging Selected Topics in Power Electronics,* vol. 7, no. 1, pp. 321-330, March 2018.

[18] I. Gonzalez-Prieto, M. J. Duran, J. J. Aciego, C. Martin, and F. Barrero, "Model predictive control of six-phase induction motor drives using virtual voltage vectors," *IEEE Transactions on Industrial Electronics,* vol. 65, no. 1, pp. 27-37, January 2017.

[19] C. Xiong, H. Xu, T. Guan, and P. Zhou, "A constant switching frequency multiple-vector-based model predictive current control of five-phase PMSM with nonsinusoidal back EMF," *IEEE Transactions on industrial Electronics,* vol. 67, no. 3, pp. 1695-1707, March 2019.

[20] M. A. Frikha, J. Croonen, K. Deepak, Y. Benômar, M. El Baghdadi, and O. Hegazy, "Multiphase motors and drive systems for electric vehicle powertrains: State of the art analysis and future trends," *Energies,* vol. 16, no. 2, p. 768, Jan 2023.

[21] D. Ronanki and S. S. Williamson, "A simplified space vector pulse width modulation implementation in modular multilevel converters for electric ship propulsion systems," *IEEE Transactions on Transportation Electrification,* vol. 5, no. 1, pp. 335-342, December 2018.

[22] K. Thantirige, A. K. Rathore, S. K. Panda, G. Jayasignhe, M. A. Zagrodnik, and A. K. Gupta, "Medium voltage multilevel converters for ship electric propulsion drives," in *2015 International Conference on Electrical Systems for Aircraft, Railway, Ship Propulsion and Road Vehicles (ESARS)*, March 2015: IEEE, pp. 1-7.

[23] M. Schweizer, T. Friedli, and J. W. Kolar, "Comparative evaluation of advanced three-phase three-level inverter/converter topologies against two-level systems," *IEEE Transactions on industrial electronics,* vol. 60, no. 12, pp. 5515-5527, December 2012.

[24] C. Xia, G. Zhang, Y. Yan, X. Gu, T. Shi, and X. He, "Discontinuous space vector PWM strategy of neutral-point-clamped three-level inverters for output current ripple reduction," *IEEE Transactions on Power Electronics,* vol. 32, no. 7, pp. 5109-5121, July 2016.

[25] G. Zhang, Y. Su, Z. Zhou, and Q. Geng, "A carrier-based discontinuous PWM strategy of NPC Three-level inverter for common-mode voltage and switching loss reduction," *Electronics,* vol. 10, no. 23, p. 3041, December 2021.

[26] F. Barrero, M. R. Arahal, R. Gregor, S. Toral, and M. J. Durán, "One-step modulation predictive current control method for the asymmetrical dual three-phase induction machine," *IEEE Transactions on Industrial Electronics,* vol. 56, no. 6, pp. 1974-1983, June 2009.

[27] M. J. Duran, J. Prieto, F. Barrero, and S. Toral, "Predictive current control of dual three-phase drives using restrained search techniques," *IEEE Transactions on Industrial Electronics,* vol. 58, no. 8, pp. 3253-3263, August 2010.

[28] M. Habibullah, D. D.-C. Lu, D. Xiao, and M. F. Rahman, "Finite-state predictive torque control of induction motor supplied from a three-level NPC voltage source inverter," *IEEE Transactions on Power Electronics,* vol. 32, no. 1, pp. 479-489, Jaunary 2016.

[29] Y. Hu, Z.-Q. Zhu, and M. Odavic, "Comparison of two-individual current control and vector space decomposition control for dual three-phase PMSM," *IEEE Transactions on Industry Applications,* vol. 53, no. 5, pp. 4483-4492, May 2017.

[30] I. Zoric, M. Jones, and E. Levi, "Vector space decomposition algorithm for asymmetrical multiphase machines," in *2017 International Symposium on Power Electronics (Ee)*, Oct. 2017: IEEE, pp. 1-6.

[31] B. Wu and M. Narimani, *High-power converters and AC drives*. John Wiley & Sons, January 2017.

[32] P. Drozdowski, "Modelling of BLDCM with a double 3-phase stator winding and back EMF harmonics," *Archives of Electrical Engineering,* vol. 64, no. 1, March 2015.

[33] M. Gu, Z. Wang, K. Yu, X. Wang, and M. Cheng, "Interleaved model predictive control for three-level neutral-point-clamped dual three-phase PMSM drives with low switching frequencies," *IEEE Transactions on Power Electronics,* vol. 36, no. 10, pp. 11618-11630, October 2021.

[34] [R. A. Raj, M. Shreelakshmi, and S. George, "Multiband hysteresis current controller for three level BLDC motor drive," in *2020 International Conference on Power, Instrumentation, Control and Computing (PICC)*, December 2020: IEEE, pp. 1-6.

[35] C. Bian, X. Li, and G. Zhao, "The peak current control of permanent magnet brushless DC machine with asymmetric dual-three phases," *CES Transactions on Electrical Machines Systems,* vol. 2, no. 1, pp. 129-135, March 2018.

[36] N. Celanovic and D. Boroyevich, "A comprehensive study of neutral-point voltage balancing problem in three-level neutral-point-clamped voltage source PWM inverters," *IEEE Transactions on power electronics,* vol. 15, no. 2, pp. 242-249, March 2000.

[37] J. Chen, Z. Wang, Y. Wang, and M. Cheng, "Analysis and control of NPC-3L inverter fed dual three-phase PMSM drives considering their asymmetric factors," *Journal of Power Electronics,* vol. 17, no. 6, pp. 1500-1511, November 2017.

[38] Ch. Xue, D. Zhou, and Y. Li, "Finite-Control-Set Model Predictive Control for Three-Level NPC Inverter-fed PMSM Drives with LC Filter," *IEEE Trans. Ind. Electron,* vol. 68, Dec. 2021.

[39] Y. Lue and C. Liu, "A Flux Constrained Predictive Control for a Six-Phase PMSM Motor With Lower Complexity," *IEEE Trans. Ind. Electron,* vol. 66, pp. 5081-5093, July 2018.

Biographies

Zahra Emami was born in Isfahan, Iran, in 1981. She received M.Sc. degrees from Isfahan University of technology, Iran. She is currently a PHD student in University of Kashan, Kashan, Iran. Her research interests include power electronics, control of electrical motor drives, Ms. Emami was the recipient of the IEEE 1th Power Electronics, Drive Systems, and Technologies Conference (PEDSTC'10) best paper award in 2010.

Abolfazl Halvaei Niasar (S'04–M'06–SM'14) was born in Kashan, Iran in 1974. He received his B.Sc., M.Sc., and Ph.D. in 1996, 1999, and 2008 from Isfahan University of Technology (IUT), University of Tehran (UT) and Iran University of Science and Technology (IUST) respectively, all in electrical engineering. He has joined the Department of Electrical and Computer Engineering at University of Kashan, Kashan, Iran since 2008 as assistant professor. He has authored more than 150 technical papers published in journals and conference proceedings. He is the holder of two Iranian patents and has directed some industrial research projects in field of electrical drives. His current major research interests include PM and brushless DC motor (BLDC) drives, sensorless drives, design, analysis and control of electrical machines. Dr. Halvaei is senior member of the Institute of Electrical and Electronics Engineers, IEEE.